Fluid-kinetic propulsive magnetic nozzle model in the fully magnetized limit

IEPC-2019-254

Presented at the 36th International Electric Propulsion Conference
University of Vienna, Austria
September 15-20, 2019

Judit Nuez*, Mario Merino† and E. Ahedo‡
Equipo de propulsión espacial y plasmas (EP2), Universidad Carlos III de Madrid (UC3M), Spain

A kinetic electron model and a fluid ion model are combined to describe the 2D plasma expansion in an axisymmetric magnetic nozzle in the fully-magnetized, collisionless limit. Electrons can be separated into free, reflected, and doubly-trapped populations, and are seen to develop anisotropy and to cool down in a non-trivial way downstream. A polytropic electron model with same asymptotic electric potential value, ϕ_∞, misses these kinetic aspects and fails to approximate the behavior of the electric potential and the average electron temperature. These differences are important in determining the performance of the device.

I. Introduction

MAGNETIC nozzles[1–3] (MNs) act as the main plasma acceleration stage of electrodeless thrusters such as the helicon plasma thruster (HPT) and the electron-cyclotron-resonance thruster (ECRT), but is it also an essential part of the applied-field magnetoplasmadynamic thruster (AFMPDT), the variable specific impulse magnetoplasma rocket (VASIMR), and other devices.[4] Understanding the plasma expansion in the guiding magnetic field of the MN is crucial to develop predictive models of the performance of these thrusters, as well as to determine the electric potential map and assess the energy and amount of plasma backflow to the spacecraft.

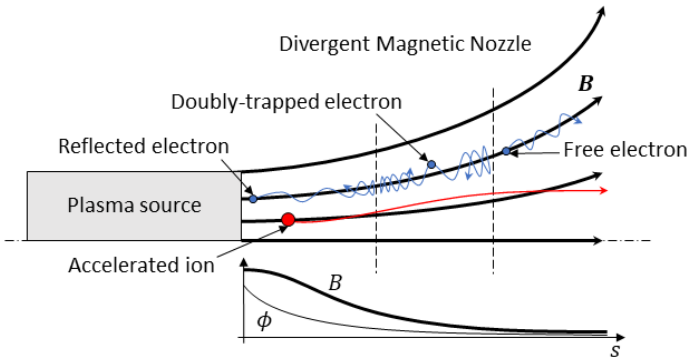

Figure 1: Sketch of a MN and typical trajectories of reflected, doubly-trapped, free electrons, and ions. The electrostatic field $-\nabla\phi$ developed in the plasma accelerates ions downstream and confines most electrons. This, combined with the magnetic mirror effect on individual particles due to the diverging magnetic field $\boldsymbol{B}$, gives rise to the existence of the different electron subpopulations.

*Aerospace Engineer
†Associate Professor, mario.merino@uc3m.es
‡Professor, eduardo.ahedo@uc3m.es

The focus of this work is on near-collisionless MN flows composed of hot, magnetized electrons and comparatively cold ions, which are relevant to (at least) HPTs and ECRTs. These flows are characterized by the set-up of a monotonically decreasing electrostatic field $-\nabla\phi$ in the plasma that accelerates ions downstream and confines most of the electrons, except for the most energetic ones (see figure 1). This field maintains the plasma quasineutrality and converts the electron internal energy into directed ion kinetic energy. The electric potential map $\phi(\boldsymbol{r})$ depends strongly on the electron thermodynamics.[5] Given the low number of collisions in the plasma, electrons are typically away from local thermodynamic equilibrium (LTE), which hinders an accurate representation of the electron species by means of otherwise convenient fluid models, since a consistent closure relation (CR) for the fluid equation hierarchy requires to account for the full kinetic electron response. Indeed, in the collisionless limit, electrons develop temperature anisotropy, and cool down in a non-trivial way due to the existence of effective potential barriers in phase space due to the interplay between electrostatic forces and magnetic mirror forces that creates empty regions and isolated, partially-populated regions in the electron velocity distribution function (EVDF).[6–9] The resulting electron behavior is far from the commonly-used isothermal or polytropic models, whose theoretical justification fails in a collisionless plasma. Accounting for the correct electron response is paramount in the study of the plasma expansion and the determination of the propulsive performance of the MN.

This paper analyzes the self-consistent cold-ion and hot-electron expansion in a 2D axisymmetric MN in the collisionless and full-magnetization limit, taking into account the kinetic electron response. The goal is to investigate the 2D kinetic behavior of the electrons, and the consequences this behavior has on the applicability of fluid electron models. The main questions to be answered are to what extent a polytropic model is a valid approximation of the kinetic model, and how important are 2D geometry effects in this validity. The problem is approached by combining two previously presented models, AKILES[10] and FUMAGNO,[11] which have both been open-sourced and are available to the community.[12,13] AKILES is a 1D kinetic plume code valid in the unmagnetized limit, which is adapted here to the fully-magnetized electron limit consistent with the formulation of.[6] It is shown that the electron equations are mathematically analogous in the two limits due to the existence of adiabatic invariants that play a similar role in either case. FUMAGNO is a 2D and 3D two-fluid code that describes the fully-magnetized expansion of a plasma in a magnetic nozzle. The code is extended here to accept the tabular kinetic results from AKILES, to yield the full 2D plasma response using an iterative approach.[14] This enables analyzing the kinetic cooling and anisotropization of electrons in the 2D domain, and extracting conclusions on the operation of the device. The fluid-kinetic results are compared against a basic polytropic electron model to show the main differences.

The rest of this contribution is organized as follows. Section II summarizes the combined 2D fluid-kinetic MN model, and describes the analogy between the fully-magnetized and unmagnetized paraxial electron kinetic models. Section III presents and discusses the simulation results. Finally, conclusions are gathered in Section IV. Advanced kinetic studies of the electron population in a MN are presented in a companion paper, reference 15.

II. Fluid-kinetic plasma model

The plasma/MN model presented here consists of a fluid ion model coupled with a kinetic electron model. The diverging, axisymmetric applied magnetic field $\boldsymbol{B}$ is assumed known, while the self-consistent electric potential map $\phi(z,r)$ and the plasma properties are found iteratively by combining both models.

A. Fluid ion model

The fully-magnetized, collisionless plasma model of reference 11 is adapted here to solve the ion flow in the MN. A full derivation of the model equations can be found in that reference. In the following, e, m_e, T_e, m_i are the electron charge, mass, and temperature, and the ion mass, while B is the magnetic field strength and R is the characteristic radius of the plasma. We shall call s the meridional coordinate along each magnetic tube or line. A subindex "0" denotes the value of a variable on a given magnetic line at the magnetic throat, e.g. B_0. These values therefore depend on the radius r_0 of that magnetic line at the throat. A double subindex "00" denotes the value at the origin of coordinates, i.e., at the center of the magnetic throat.

In the collisionless, steady-state, fully-magnetized limit, the ion gyrofrequency satisfies[11,16]

$$\Omega_i R/c_s = eBR/\sqrt{T_e m_i} \gg 1, \tag{1}$$

and all drift velocities are much smaller than the sonic velocity $c_s = \sqrt{T_e/m_i}$, so, to first approximation, the ion fluid velocity is parallel to the applied magnetic field $\boldsymbol{u}_i = u_i \mathbf{1}_\parallel$. The cold, singly-charged ions follow the magnetic tubes, along which their fluid equations take the simple integral form:

$$n_i u_i / B = G_i(\psi); \qquad \frac{1}{2} m_i u_i^2 + e\phi = H_i(\psi). \tag{2}$$

where $G_i(\psi)$ and $H_i(\psi)$ are integration constants on each magnetic tube, labeled by the streamfunction ψ, and all other symbols are conventional. Once boundary conditions $n_i = n_{i0}$, $u_i = u_{i0}$ are given at the magnetic throat $s = 0$ for each magnetic tube, these expressions suffice to determine the ion properties n_i and u_i as a function of $B(s)/B_0$, the local magnetic field strength normalized with its value at $s = 0$, $B_0 = B(0)$.

B. Kinetic electron model

The reader is directed to references 6 and 10 for a full account of the 1D kinetic electron model in the magnetized and the unmagnetized limits. Below, only a summary of the main aspects of the model and its generalization to 2D are given for self-completeness. Appendix A presents the analogies between the fully unmagnetized and fully magnetized models of these references.

Consider the steady-state, collisionless electron flow in a 2D, axisymmetric, slowly diverging MN. In the limit of small electron Larmor radius $\ell_e/R = \sqrt{T_e m_e}/(eBR) \ll 1$ electrons are well-magnetized and all drift velocities are small compared to the thermal velocity (note that this condition is automatically satisfied if (1) is true). Then, to first approximation the electron macroscopic velocity is parallel to the magnetic field, $\boldsymbol{u}_e = u_e \mathbf{1}_\parallel$, and in the collisionless limit, electrons remain on their respective magnetic tubes. On each magnetic tube, the distribution functions of down-marching and up-marching electrons, f_e^+ and f_e^-, are assumed to be uniform in the gyrophase angle α and the azimuthal angle θ, and to depend only on the coordinate s along the magnetic tube, the mechanical energy $E = m_e(v_\parallel^2 + v_\perp^2)/2 - e\phi$, and the magnetic moment $\mu = m_e v_\perp^2/(2B)$,

$$f_e^+ = f_e^+(s, E, \mu); \qquad f_e^- = f_e^-(s, E, \mu). \tag{3}$$

Mechanical energy E is a conserved quantity of electron motion, and μ is an adiabatic invariant that can be considered conserved in gyro-average to second order[17] in $\varepsilon = \ell_e |\partial \ln B/\partial s| \ll 1$. Hence, the kinetic equation for f_e can be written in first approximation as

$$v_\parallel \frac{\partial f_e}{\partial s} = 0. \tag{4}$$

This equation states that f_e^+ and f_e^- are propagated as constants along s for each E, μ, as long as $v_\parallel \neq 0$. The condition $v_\parallel = 0$ indicates the turning points for the electron trajectories. Expressed in terms of E, μ and the electric potential and the magnetic field strength along the magnetic tube, $\phi(s)$ and $B(s)$, this condition reads

$$E + e\phi(s) - \mu B(s) = 0. \tag{5}$$

Equation (5) may be interpreted as the definition of the *effective potential* $U_{\text{eff}}(s, \mu) = -e\phi(s) + \mu B(s)$ for the motion of the electrons along the magnetic tube. This equation subdivides the electron phase space into four distinct regions:

1. For each μ, those electrons with high enough E overcome all barriers of U_{eff} and travel between the plasma source (located at $s = 0$) and infinity downstream ($s = \infty$). These regions of phase space connect with both boundary conditions, and the source electrons in them are termed *free electrons*.
2. Those regions of phase space (s, E, μ) connected with $s = 0$ but not connected with $s = \infty$ are populated by *reflected electrons*. The reflection at the turning point surface ensures that $f_e^+ = f_e^-$.
3. Similarly, those regions of phase space connected with $s = \infty$ but not connected with $s = 0$ may only be occupied by *backstreaming electrons* from the ambient, if any. As before, reflection ensures that $f_e^+ = f_e^-$ in this region.
4. Finally, there can be isolated regions of existence, not connected to either boundary. *Doubly-trapped* electron populations can occupy these regions of phase space. In this region, reflection also enforces $f_e^+ = f_e^-$.

The electron model is closed by the boundary conditions for f_e^+ and f_e^- at $s = 0$ and $s = \infty$, respectively. For simplicity, at $s = 0$, a semi-Maxwellian population of reference density n_e^* and temperature T_e^* is considered for f_e^+,

$$f_{e0}\mathrm{d}v^3 = n_e^* \left(\frac{m_e}{2\pi T_e^*}\right)^{3/2} \exp\left(-\frac{E}{T_e^*}\right) \mathrm{d}v^3. \tag{6}$$

With regards to the condition at $s = \infty$, this study does not consider backstreaming electrons, and therefore, regions of type 3 in the list above will be *empty regions* with $f_e^+ = f_e^- = 0$.

While these boundary conditions determine unambiguously the EVDF in regions 1–3, the isolated regions of type 4 can hold an arbitrary distribution function in this steady-state model. The filling of these regions can occur during the transient thruster ignition[9] or be caused by infrequent but non-zero collisions. The latter mechanism suggests that in these regions an essentially-thermalized population (with itself and with neighboring regions of phase space) will exist after sufficiently long times. In this study, these regions are considered to be populated with the same distribution function as upstream, i.e., a Maxwellian population of reference density n_e^* and temperature T_e^*.

It turns out that the spatial dependence of the model on s along each diverging magnetic tube can be expressed in terms of B by inverting the relation $B = B(s)$. Once $f_e^+(B)$ and $f_e^-(B)$ are known everywhere, any moment $\mathcal{M}_{ij}$ of the distribution function, and in particular n_e, u_e, can be computed via direct integration. This integration can be carried out in $(v_\parallel, v_\perp)$ space, or alternatively, in (E, μ) space after applying the necessary coordinate transformations:

$$\mathcal{M}_{ij} = 2\pi \int \mathrm{d}v_\parallel \mathrm{d}v_\perp f_e v_\parallel^i v_\perp^{j+1} = \frac{\pi B}{m_e}\left(\frac{2}{m_e}\right)^{\frac{i+j+1}{2}} \int \mathrm{d}E\mathrm{d}\mu [f_e^+ + (-1)^i f_e^-](E - \mu B + e\phi)^{\frac{i-1}{2}} (\mu B)^{\frac{j}{2}}, \tag{7}$$

Observe that only free electrons contribute to odd moments in $v_\parallel$. Finally, the relevant magnitudes for this study, are defined below:

$$\begin{aligned}
&n_e = \mathcal{M}_{00} && u_e = \mathcal{M}_{10}/n_e && \\
&T_{\parallel e} = m_e(\mathcal{M}_{20}/n_e - u_e^2) && T_{\perp e} = m_e\mathcal{M}_{02}/(2n_e) && T_e = (T_{\parallel e} + 2T_{\perp e})/3 \\
&q_{\parallel e} = (m_e\mathcal{M}_{30} - m_e n_e u_e^3 - 3n_e u_e T_{\parallel e})/2 && q_{\perp e} = m_e\mathcal{M}_{12}/2 - n_e u_e T_{\perp e} && q_e = q_{\parallel e} + q_{\perp e},
\end{aligned}$$

where all symbols are conventional. Note that $q_{\parallel e}$, $q_{\perp e}$ are parallel heat fluxes of parallel and perpendicular thermal energy, respectively, while q_e is the parallel heat flux of total thermal energy.

C. Iterative solution method

As noted before, on each magnetic tube ion and electron properties depend on the coordinate s only through the value of the local magnetic field strength, $B(s)/B_0$. The ion and electron models along a single magnetic tube can be normalized to remove the dependency on B_0, n_{i0}, u_{i0}, n_e^* and T_e^*, values which are naturally tube-dependent. This conveniently enables solving the coupled model in 1D to obtain ϕ and the plasma properties as a function of B/B_0, and then rescaling this solution to each magnetic tube to obtain the 2D solution.

Therefore, the iterative solution procedure is as follows. The potential is fixed $\phi = 0$ at the magnetic throat plane. Given an initial guess of $\phi(B)$ along a generic magnetic line $B(s)$, the ion model is used to compute $n_i(B), u_i(B)$, and the electron model to compute $n_e(B), u_e(B)$. The ion sonic flow condition on the whole throat plane is imposed at each iteration. Quasineutrality and current-free conditions are then checked for that guess of $\phi(B)$, demanding that the solution satisfies:

$$n_i(B) = n_e(B); \qquad\qquad n_i(B)u_i(B) = n_e(B)u_e(B), \tag{8}$$

for all points on the magnetic line (the last expression needs only be imposed at one location to be automatically fulfilled everywhere else). The information on the error committed by the guessed $\phi(B)$ profile is then used to update the guess, and the process is repeated until the global error is below a chosen tolerance.

Once the self-consistent solution has been found, other moments of the EVDF can be computed to analyze the kinetic electron response in the MN. Incidentally, observe that the kinetic model allows for other conditions than in equation (8) to be imposed. In particular, there exists a whole class of solutions without zero net current, which can be relevant in future studies.

III. Results and discussion

A. 1D analysis

The solution of the model for initially sonic Xenon ions ($M_{i0} = u_{i0}/c_{s0} = 1$, $\mu = \sqrt{m_i/m_e} = 491.689$, $\chi = u_{i0}/\sqrt{T_e^*/m_e} = 0.002$, for comparison with reference 10) is discussed next. The normalized solution of $\phi(B)$ along a generic magnetic line is shown in figure 2. The electric potential undergoes a quick initial fall. At $B/B_0 = 0.01$, the relative difference $(\phi - \phi_\infty)/\phi_\infty$ is already around 1.6% only. Then, it tends to the asymptotic value $\phi_\infty = -7.4T_{e0}/e$. Observe that T_{e0} and n_{e0} are unknown a priori, and must be computed as part of the solution. In the present case, $T_{e0} = 0.995T_e^*$ and $n_{e0} = 0.999n_e^*$.

It is possible to define a polytropic electron model that yields the same total potential fall ϕ_∞ along the nozzle,

$$\gamma = \frac{|e\phi_\infty|}{|e\phi_\infty| - T_{e0}(0)} = 1.155 \tag{9}$$

The fluid/fluid FUMAGNO solution for this polytropic electron model has also been plotted on figure 2 for comparison. While both models tend to ϕ_∞, it is clear that the polytropic model does so at a slower rate. Consequently, the polytropic model tends to underestimate the rate of ion acceleration in the MN. While the asymptotic value is identical in both models (by our choice of γ), this discrepancy affects most of the near-region plasma expansion, where thrust is generated and the high magnetization of the MN holds. Thus, invoking a polytropic approximation, even if chosen consistently with the final asymptotic behavior of the plasma plume, might have an important effect on the calculation of the MN performance figures like thrust, specific impulse, divergence and conversion efficiencies, etc. in practice, when only a finite length of nozzle is investigated.

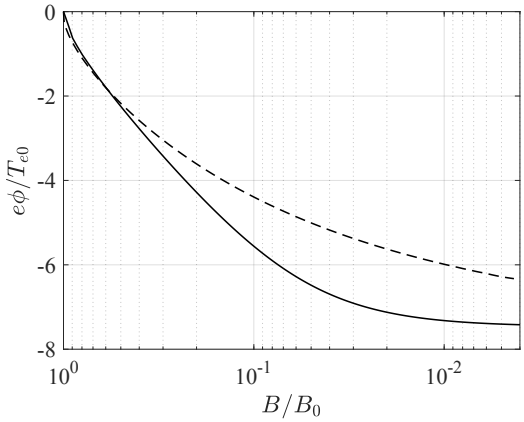

Figure 2: Solution of the electric potential as a function of the local magnetic field strength, $e\phi(B/B_0)/T_{e0}$, using the kinetic electron model (solid line) and the polytropic electron model with same ϕ_∞ (dashed line).

The corresponding normalized electron moments in the divergent MN are displayed on figures 3 and 4. In the case of the average temperature T_e, the results from the polytropic model are also shown for comparison. As it can be observed, the major contributor to even electron moments is at first the reflected electron population, and soon in the expansion, the doubly-trapped electrons begin to dominate. Odd moments, on the other hand, only have the contribution of free electrons. The electron bulk velocity increases downstream in the same manner as the ion velocity; note that the ion properties satisfy $n_i = n_e$ and $u_i = u_e$ according to equation (8). These trends agree with those previously reported in 6, 18.

The electron parallel and perpendicular temperature components behave differently in the MN, giving rise to the development of electron anisotropy. While it cannot be appreciated in figure 4, $T_{\parallel e}$ goes to a non-zero asymptotic value far downstream, while $T_{\perp e}$ goes to zero.[6] This anisotropy is missed by the polytropic model.

The average temperature T_e in the kinetic solution is nearly constant in the initial part of the expansion (roughly down to $B/B_0 = 0.1$), but then cools down gradually. This suggests the possibility of approximating the average temperature behavior by two simpler patched fluid models.

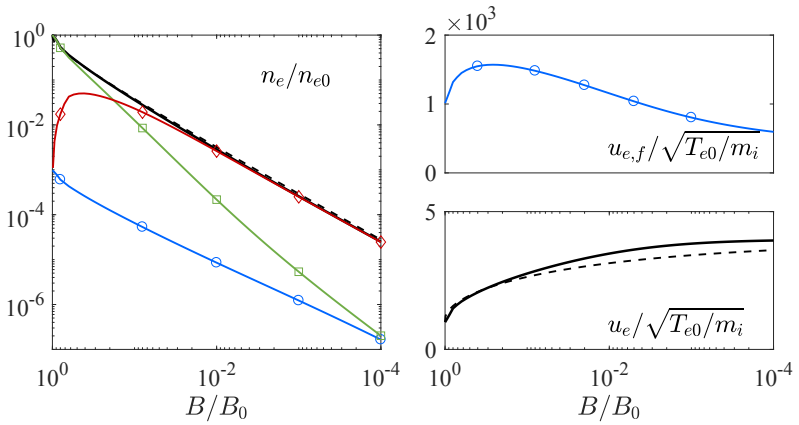

Figure 3: Normalized electron density n_e and electron velocity u_e as a function of B/B_0 for a generic magnetic line. The density and velocity of each electron subpopulation alone are shown. Thin lines represent free (blue circles), reflected (green squares) and doubly-trapped (red diamonds) electrons. The thick black line represents the whole electron population with the kinetic model. The dashed line indicates the solution of the polytropic model with same ϕ_∞ for comparison.

The parallel and perpendicular heat fluxes exhibit different sign, and the sign of the total heat flux q_e changes along the expansion. The fluxes of the free electrons alone and the whole electron population differ due to the different density, velocity, and temperature values for the free subpopulation and for the whole species (see the definitions of $q_{\parallel e}, q_{\perp e}, q_e$ in Section B). The heat flux q_e for the approximated polytropic model has been computed from the paraxial energy equation, neglecting electron inertia and anisotropy, and taking $q_e/B \to 0$ far downstream to remove the additive constant:[5]

$$q_e = n_e u_e T_e \left(\frac{\gamma}{\gamma - 1} - \frac{5}{2} \right) \quad \text{(Polytropic model)} \tag{10}$$

As it can be observed, the polytropic total heat flux is essentially proportional to the pressure $n_e T_e$, and misses the complexity of the kinetic solution.

B. 2D analysis

The 1D solution for a generic magnetic line has been used to generate the electron response of a 2D axisymmetric MN flow with an initially Gaussian density profile that drops 3 orders of magnitude radially, given by

$$n_e(0,r) = n_{e0}(r) = n_{e00} \exp[-(\ln 10^3) r^2/R^2] \qquad \text{for: } r \leqslant 1; \text{ else, } n_e(0,r) = 0, \tag{11}$$
$$T_e(0,r) = T_{e0}(r) = T_{e00}, \tag{12}$$
$$u_i(0,r) = c_s(0,r), \tag{13}$$
$$\phi(0,r) = 0. \tag{14}$$

The magnetic field of a single magnetic loop located at the origin is used. The resulting maps of electron potential ϕ, electron density n_e, electron temperatures $T_{\parallel e}$, $T_{\perp e}$, T_e and electron parallel heat fluxes $q_{\parallel e}$, $q_{\perp e}$, q_e are shown in figures 5, 6, and 7 down to the very far expansion region ($z = 300R$).

Figure 5 shows the quicker drop of ϕ in the kinetic model toward the asymptotic value ϕ_∞ than the polytropic model, consistent with figure 2. As a consequence of this difference, the gain of ion velocity in the kinetic model is faster. Of course, the final asymptotic value, related to ϕ_∞, is identical in both models.

Figure 6 shows the evolution of the electron density in the MN and the relative contributions of each electron population (free, reflected, and doubly-trapped) to the electron density n_e. As it can be seen, free

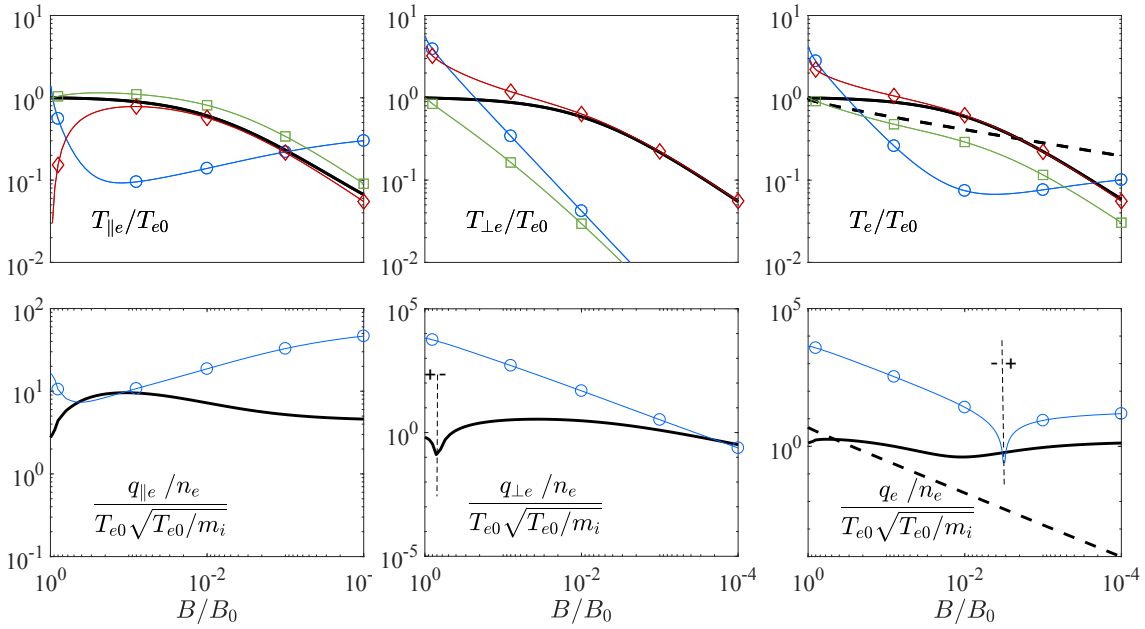

Figure 4: Normalized moments of the electron velocity distribution function as a function of B/B_0: $T_{\parallel e}$, $T_{\perp e}$, T_e $q_{\parallel e}$, $q_{\perp e}$, and q_e for the magnetic line at $r_0/R = 0$. The moments of each electron subpopulation alone are shown. Thin lines represent free (blue circles), reflected (green squares) and doubly-trapped (red diamonds) electrons. The change of sign of q_e of free electrons is marked in the plot. The thick line represents the whole electron population. Where present, the dashed line indicates the solution of the polytropic model with same ϕ_∞ for comparison.

electrons are a minority everywhere, and provide the neutralizing current for the escaping ions. Initially, reflected electrons abound, but doubly-trapped electrons dominate the far region. The uncertainties of the kinetic model in the characterization of this subpopulation are therefore important downstream; future work will improve their description by adding incipient collisionality to the model.

Figure 7 depicts the anisotropy ratio $T_{\perp e}/T_{\parallel e}$, and the average temperature T_e for the kinetic and polytropic models. While the electrons start as an isotropic species (according to our boundary condition at the MN throat), it is evident that anisotropy develops far downstream. However, while the anisotropy ratio goes to zero at infinity, it is still close to unity for a large part of the MN (at $z = 100R$, $T_{\perp e}/T_{\parallel e} \simeq 90\%$).

Figure 7 also shows the heat fluxes divided by the density, $q_{\parallel e}/n_e$, $q_{\perp e}/n_e$, q_e/n_e. In agreement with the 1D results of figure 4, $q_{\parallel e}/n_e$ and $q_{\perp e}/n_e$ vary about one order of magnitude along the expansion, and have opposite signs for most of the MN, while the total heat flux q_e/n_e has a non-monotonic behavior along each magnetic tube.

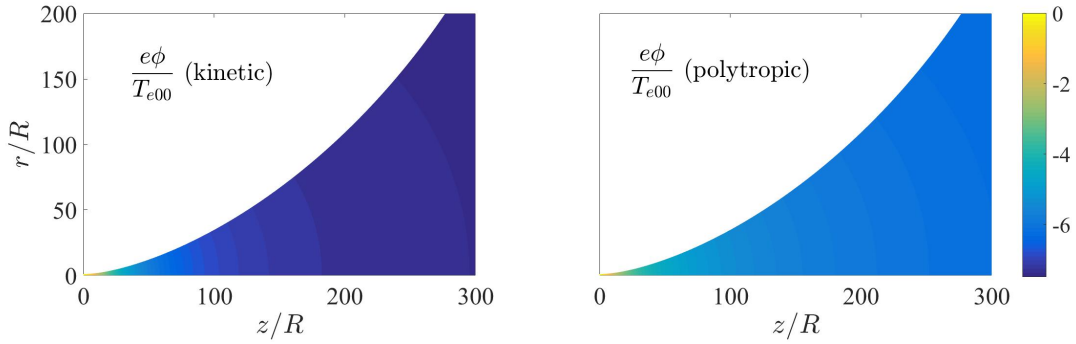

Figure 5: 2d map the electric potential with kinetic model (left) and the polytropic model (right).

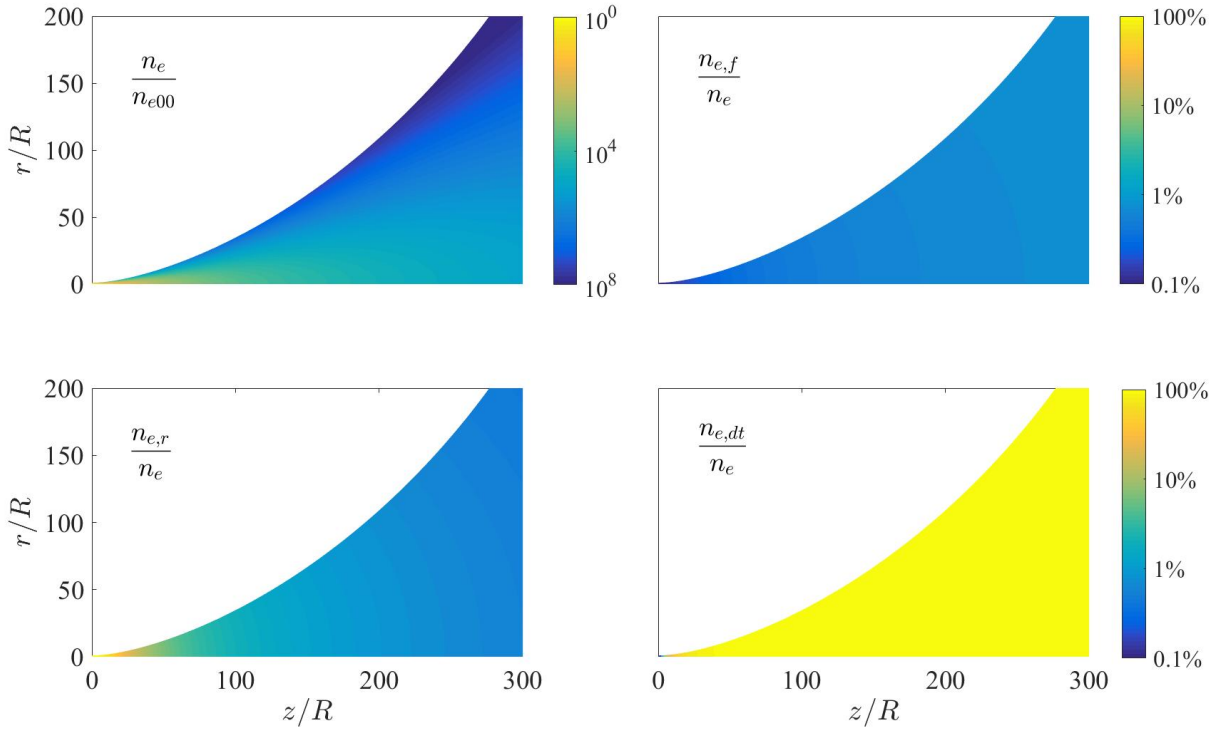

Figure 6: 2D map of the total electron density in the MN, and the fraction of n_e due to the free ($n_{e,f}$), reflected ($n_{e,r}$), and doubly-trapped ($n_{e,dt}$) electron subpopulations.

The azimuthal electron current is central to the operation of the MN, since it is responsible of the generation of a radially-confining and axially-accelerating magnetic force density on the plasma, $j_{\theta e}B_z$ and $-j_{\theta e}B_r$, respectively.[19] The integrated reaction to the latter force density component is felt on the thruster magnetic field generator and gives rise to magnetic thrust. While $j_{\theta e}$ is vanishingly small in the high-magnetization limit, the force densities $j_{\theta e}B_z$ and $-j_{\theta e}B_r$ are finite and can be obtained from the electron momentum equation,

$$j_{\theta e}B = -\frac{\partial(n_e T_{\perp e})}{\partial \mathbf{1}_\perp} + e n_e \frac{\partial \phi}{\partial \mathbf{1}_\perp} \tag{15}$$

These force densities are a purely 2D phenomenon, and are plotted on figure 8. The perpendicular pressure gradient is maximal at the MN throat, and decreases downstream, while each of the magnetic field components behaves differently: Along $r = \text{const}$ lines, B_z decreases monotonically, but B_r increases from zero at the throat to reach a maximum and then decrease. Consequently, the axial force density exhibits a maximum value in the near plume region. This is where most of the ion acceleration takes place, and where most of the magnetic thrust is generated, in agreement with reference 20. The radial force density that confines the plasma in the MN is greater than the axial force density, and is larger at the throat, and decreases downstream.

IV. Conclusion

The open-sourced kinetic AKILES model and fluid FUMAGNO model have been coupled together to provide a fluid/kinetic description of the 2D plasma expansion in an axisymmetric magnetic nozzle in the fully-magnetized, collisionless limit. The resulting model has the same features as the 1D kinetic model for each magnetic line, which simplifies the iterative solution process.

Electrons, which can be divided into free, reflected, and doubly-trapped populations, do not follow any simple closure relation, and their temperature and the electric potential are not approximated well by simple polytropic models even if the same asymptotic value of the potential, ϕ_∞, is chosen. This conclusion can

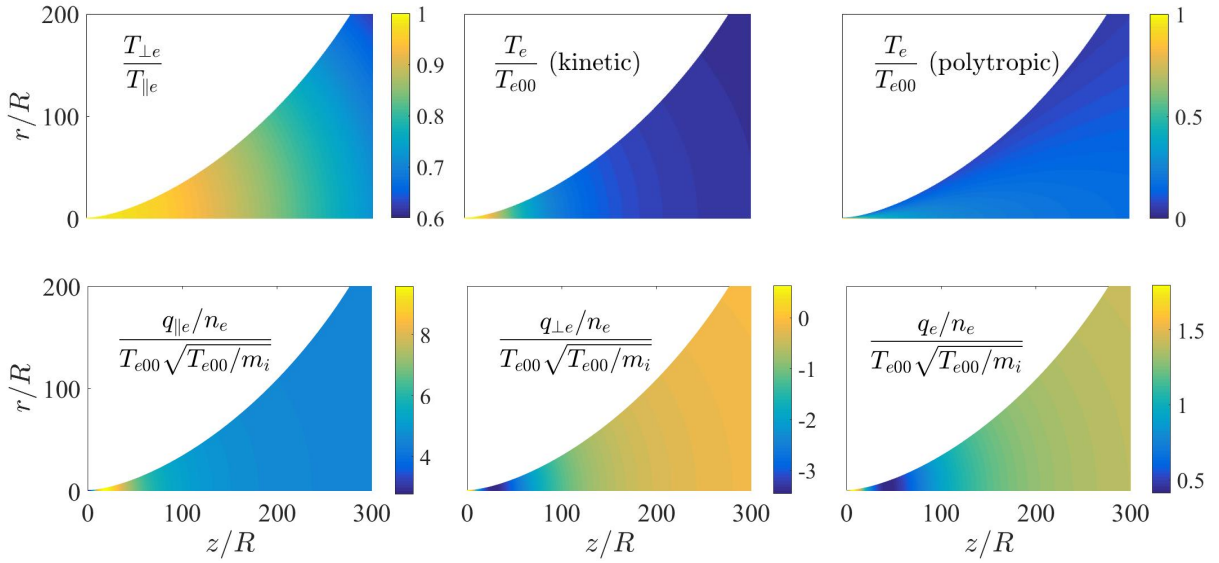

Figure 7: 2D maps of electron anisotropy ratio $T_{\perp e}/T_{\parallel e}$ (left) and average temperature T_e in the kinetic model (center). The temperature of electrons in the polytropic model is shown for comparison (right). The temperature at the origin (T_{e00}) has been used to normalize the last two plots.

be already extracted from a 1D analysis, and is equally evident in the 2D results. Electrons develop a mild anisotropy that grows downstream, and exhibit no-trivial kinetic heat fluxes that are missed completely by the simpler fluid models. These kinetic effects may have an important effect in the calculation of the magnetic nozzle performance, such as the magnetic thrust generated, whose density was computed using the 2D plasma profiles.

Doubly-trapped electrons are seen to become the dominant population downstream. The present kinetic model makes the ansatz that these regions of phase space are populated with the same distribution function as upstream; this assumption must be revised in future work. A way around the indeterminacy of doubly-trapped electrons is to include small but non-zero collisionallity in the model, and/or to deal with the transient plume set-up process.

Future lines of research can also study the effect of a background plasma, whose electrons would backstream into the magnetic nozzle and affect the expansion. This study is straightforward with the current model. Additionally, it is also possible to adapt the 2D AKILES/FUMAGNO model to 3D magnetic nozzles and study directional thrust, relevant for thrust-vector-control magnetic nozzles.[16]

Clearly, present results are limited by the full-magnetization assumption of ions, which is typically not met in actual devices for current magnetic field strengths and propellant types, except perhaps in the near expansion region. Lifting this assumption requires a different iterative solution approach for the model, as now the plasma properties on all magnetic lines must be solved simultaneously. This effort will be initiated

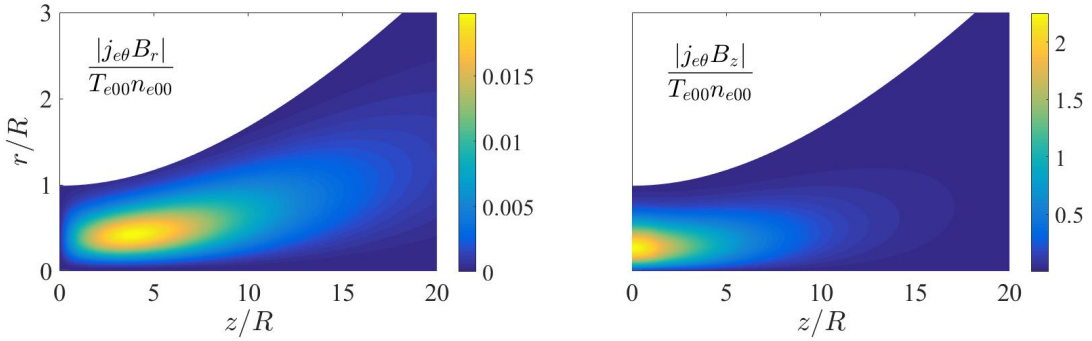

Figure 8: 2D maps of the axial magnetic force density $-j_{\theta e}B_r$ (left) and radial magnetic force density $j_{\theta e}B_z$ (right), normalized with T_{e00} and n_{e00}, the values at the origin.

soon by combining AKILES with the partially-magnetization magnetic nozzle code, DIMAGNO.[21]

Appendix

A. Analogy between fully-magnetized and unmagnetized electron models

It is instructive to compare this magnetized electron model with the unmagnetized model of reference 10, to see the similarities and analogies between the two limit regimes. In the unmagnetized model, electrons conserve their mechanical energy E and the canonical angular momentum about the plume axis, $p_\theta = m_e r v_\theta$. To close the problem, an additional assumption is needed in this case on the electric potential profile in the radial direction. An arguably reasonable hypothesis is that the potential has a parabolic shape in this direction, and can be given as

$$\phi(z,r) = -\frac{T_e^* h_0^2}{e h^4(z)} r^2 + \phi_z(z), \tag{16}$$

where $h(z)$ is a function that represents the radius of the plasma beam (with $h_0 = h(0)$) and $\phi_z(z)$ is the potential along the plume axis. Provided that ϕ_z is slowly varying, the radial action integral J_r of each individual electron is an adiabatic invariant of motion that is conserved in average to second order,

$$J_r = \oint m_e v_r \mathrm{d}r. \tag{17}$$

Similarly to the magnetized case along a single magnetic tube, the evolution of the phase-averaged EVDF parametrized in terms of (z, E, J_r, p_θ) is given by an expression analogous to equation (4), and the axial electron dynamics is governed by the effective potential $U_{\mathrm{eff}}(z, p_\perp) = -e\phi_z(z) + \sqrt{2T_e^*/m_e} h_0 p_\perp / h^2$, where $p_\perp = J_r/\pi + |p_\theta|$. Therefore, both kinetic models are analogous if the following identifications are made:

$$\frac{B}{B_0} \quad \leftrightarrow \quad \frac{h_0^2}{h^2} \tag{18}$$

$$\frac{\mu}{T_e^*/B_0} \quad \leftrightarrow \quad \sqrt{2}\frac{J_r/\pi + |p_\theta|}{h_0\sqrt{m_e T_e^*}}. \tag{19}$$

Acknowledgments

The research leading to these results has received funding from the European Union H2020 Program under grant agreement number 730028 (Project MINOTOR). Additional funding came from Project ESP2016-75887 (Spain's National Research and Development Plan - MINECO/FEDER).

References

[1]Gerwin, R., Marklin, G., Sgro, A., and Glasser, A., "Characterization of plasma flow through magnetic nozzles," Tech. Rep. AFSOR AL-TR-89-092, Los Alamos National Laboratory, 1990.

[2]Ahedo, E. and Merino, M., "Two-dimensional supersonic plasma acceleration in a magnetic nozzle," *Physics of Plasmas*, Vol. 17, No. 7, 2010, pp. 073501.

[3]Merino, M. and Ahedo, E., "Magnetic Nozzles for Space Plasma Thrusters," *Encyclopedia of Plasma Technology*, edited by J. L. Shohet, Vol. 2, Taylor and Francis, 2016, pp. 1329–1351.

[4]Ahedo, E., "Plasmas for space propulsion," *Plasma Physics and Controlled Fusion*, Vol. 53, No. 12, 2011, pp. 124037.

[5]Merino, M. and Ahedo, E., "Influence of Electron and Ion Thermodynamics on the Magnetic Nozzle Plasma Expansion," *IEEE Transactions on Plasma Science*, Vol. 43, No. 1, Jan 2015, pp. 244–251.

[6]Martínez-Sánchez, M., Navarro-Cavallé, J., and Ahedo, E., "Electron cooling and finite potential drop in a magnetized plasma expansion," *Physics of Plasmas*, Vol. 22, No. 5, 2015, pp. 053501.

[7]Little, J. and Choueiri, E., "Electron Cooling in a Magnetically Expanding Plasma," *Physical Review Letters*, Vol. 117, No. 22, 2016, pp. 225003.

[8]Hu, Y. and Wang, J., "Fully kinetic simulations of collisionless, mesothermal plasma emission: Macroscopic plume structure and microscopic electron characteristics," *Physics of Plasmas*, Vol. 24, No. 3, 2017, pp. 033510.

[9]Sánchez-Arriaga, G., Zhou, J., Ahedo, E., Martínez-Sánchez, M., and Ramos, J. J., "Kinetic features and non-stationary electron trapping in paraxial magnetic nozzles," *Plasma Sources Science and Technology*, Vol. 27, No. 3, 2018, pp. 035002.

[10]Merino, M., Mauriño, J., and Ahedo, E., "Kinetic electron model for plasma thruster plumes," *Plasma Sources Science and Technology*, Vol. 27, No. 3, 2018, pp. 035013.

[11]Merino, M. and Ahedo, E., "Fully magnetized plasma flow in a magnetic nozzle," *Physics of Plasmas*, Vol. 23, No. 2, 2016, pp. 023506.

[12]Merino, M. and Mauriño, J., "AKILES code: Advanced Kinetic Iterative pLasma Expansion Solver 2D," DOI: 10.5281/zenodo.1098432, 2017.

[13]Merino, M., "FUMAGNO code: Fully-magnetized Magnetic Nozzle simulator," DOI: 10.5281/zenodo.593787, 2017.

[14]Ramos, J., Merino, M., and Ahedo, E., "Three dimensional fluid-kinetic model of a magnetically guided plasma jet," *Physics of Plasmas*, Vol. 25, No. 6, 2018, pp. 061206.

[15]Correyero, S., Merino, M., and Ahedo, E., "Effect of the initial VDFs in magnetic nozzle expansions," 36^{th} *International Electric Propulsion Conference*, No. IEPC-2019-818, Electric Rocket Propulsion Society, Vienna, Austria, 2019.

[16]Merino, M. and Ahedo, E., "Contactless steering of a plasma jet with a 3D magnetic nozzle," *Plasma Sources Science and Technology*, Vol. 26, No. 9, 2017, pp. 095001.

[17]Goldstein, H., Poole, C. P., and Safko, J. L., *Classical mechanics*, Pearson, 2001.

[18]Navarro-Cavallé, J., Martínez-Sánchez, M., and Ahedo, E., "Collisionless electron cooling in a magnetic nozzle," *50th AIAA/ASME/SAE/ASEE Joint Propulsion Conference & Exhibit*, No. AIAA 2014-4028, American Institute of Aeronautics and Astronautics, Cleveland, Ohio, 2014.

[19]Ahedo, E. and Merino, M., "On plasma detachment in propulsive magnetic nozzles," *Physics of Plasmas*, Vol. 18, No. 5, 2011, pp. 053504.

[20]Merino, M. and Ahedo, E., "Simulation of plasma flows in divergent magnetic nozzles," *IEEE Transactions on Plasma Science*, Vol. 39, No. 11, 2011, pp. 2938–2939.

[21]Merino, M., "DIMAGNO code: Divergent Magnetic Nozzle plasma flow solver," DOI: 10.5281/zenodo.1257295, 2017.